REPORT DOCUMENTATION PAGE

Form Approved
OMB No. 0704-0188

1. AGENCY USE ONLY (Leave blank)	2. REPORT DATE	3. REPORT TYPE AND DATES COVERED
	August 1993	Professional Paper

4. TITLE AND SUBTITLE

CONCOMITANT ALTERATIONS OF DESMOSOMES, ADHESIVENESS, AND DIFFUSION THROUGH GAP JUNCTION CHANNELS IN A RAT OVARIAN TRANSFORMATION MODEL SYSTEM

5. FUNDING NUMBERS

In-house funding

6. AUTHOR(S)

L. S. Stein, D. W. J. Stein, J. Echols, R. C. Burghardt

7. PERFORMING ORGANIZATION NAME(S) AND ADDRESS(ES)

Naval Command, Control and Ocean Surveillance Center (NCCOSC)
RDT&E Division
San Diego, CA 92152-5001

8. PERFORMING ORGANIZATION REPORT NUMBER

9. SPONSORING/MONITORING AGENCY NAME(S) AND ADDRESS(ES)

Naval Command, Control and Ocean Surveillance Center (NCCOSC)
RDT&E Division
San Diego, CA 92152-5001

10. SPONSORING/MONITORING AGENCY REPORT NUMBER

11. SUPPLEMENTARY NOTES

12a. DISTRIBUTION/AVAILABILITY STATEMENT

Approved for public release; distribution is unlimited.

13. ABSTRACT (Maximum 200 words)

Gap junctional intercellular communication (GJIC), desmosomes, and cell movement were evaluated in a rat ovarian epithelial cell model system which consisted of an immortalized clonal cell line (SIGC), a pSV3neotransfected clonal derivative (SV-SIGC), and a nude mouse SV-SIGC-tumor-derived cell line (T-SV-SIGC). Complementary ultrastructural, indirect immunofluorescence, and Western blot data identified a relatively small loss of desmosomes and associated cytokeratins in SV-SIGC compared to SIGC but a near total loss in T-SV-SIGC. SIGC and SV-SIGC migrated outward from monolayer-coated microcarrier beads as epithelial sheets, whereas in T-SV-SIGC there was dissociation and migration of individual fibroblastoid cells. GJIC was assessed by fluorescence recovery after photobleaching (gap FRAP) and equations based on Fick's first law of diffusion were derived to quantitatively compare GJIC of systems with different recovery equilibria after photobleaching. Taken together the data suggested that GJIC in SIGC was quantitatively reduced to similar levels by various conditions associated with reduced cell-cell adhesiveness including transformation to T-SV-SIGC, mitosis, and culture in low calcium medium. These results supported linkage between changes in desmosomal adhesiveness, cell movement, and GJIC.

Published in *Journal of Experimental Cell Research*, 1993, Vol. 207, pp. 19-32.

14. SUBJECT TERMS	15. NUMBER OF PAGES
Gap Junctional Intercellular Communication (GJIC) Desmosomes Cell Movement	16. PRICE CODE

17. SECURITY CLASSIFICATION OF REPORT	18. SECURITY CLASSIFICATION OF THIS PAGE	19. SECURITY CLASSIFICATION OF ABSTRACT	20. LIMITATION OF ABSTRACT
UNCLASSIFIED	UNCLASSIFIED	UNCLASSIFIED	SAME AS REPORT

21a NAME OF RESPONSIBLE INDIVIDUAL	21b TELEPHONE (Include Area Code)	21c OFFICE SYMBOL
D. Stein	(619) 553-2533	Code 761

EXPERIMENTAL CELL RESEARCH 207, 19–32 (1993)

Concomitant Alterations of Desmosomes, Adhesiveness, and Diffusion through Gap Junction Channels in a Rat Ovarian Transformation Model System[1]

LISA S. STEIN,*†[2] DAVID W. J. STEIN,‡ JANA ECHOLS,† AND ROBERT C. BURGHARDT†

*Department of Pediatrics, University of California at San Diego, M-609A, 9500 Gilman Drive, La Jolla, California 92093; †Department of Veterinary Anatomy and Public Health, Texas A&M University, College Station, Texas 77843; and ‡Code 761, Naval Command, Control and Ocean Surveillance Center, Naval Research, Development, Test and Evaluation, San Diego, California 92152

Gap junctional intercellular communication (GJIC), desmosomes, and cell movement were evaluated in a rat ovarian epithelial cell model system which consisted of an immortalized clonal cell line (SIGC), a pSV3neo-transfected clonal derivative (SV-SIGC), and a nude mouse SV-SIGC-tumor-derived cell line (T-SV-SIGC). Complementary ultrastructural, indirect immunofluorescence, and Western blot data identified a relatively small loss of desmosomes and associated cytokeratins in SV-SIGC compared to SIGC but a near total loss in T-SV-SIGC. SIGC and SV-SIGC migrated outward from monolayer-coated microcarrier beads as epithelial sheets, whereas in T-SV-SIGC there was dissociation and migration of individual fibroblastoid cells. GJIC was assessed by fluorescence recovery after photobleaching (gap FRAP) and equations based on Fick's first law of diffusion were derived to quantitatively compare GJIC of systems with different recovery equilibria after photobleaching. Taken together the data suggested that GJIC in SIGC was quantitatively reduced to similar levels by various conditions associated with reduced cell–cell adhesiveness including transformation to T-SV-SIGC, mitosis, and culture in low calcium medium. These results supported linkage between changes in desmosomal adhesiveness, cell movement, and GJIC.

INTRODUCTION

The acquired ability of individual transformed cells to disseminate from a population has been considered to be an essential feature of metastasis [for review see 1]. Decreased intercellular adhesiveness is thought to play a role in the detachment and migration of epithelial cells away from an original site during the multistep process of cellular transformation leading to metastasis [2]. Although it is unlikely that changes in any one adhesive component can explain the complex adhesive interactions that occur during progression [1], it has been suggested that alterations in functional adhesive properties could arise in part through the loss of intercellular junctions [2, 3].

Desmosomes are punctate intercellular junctions which often occur adjacent to gap junctions in normal epithelium [4, 5]. They are considered to play a key role in epithelial cell adhesion by binding cells together and linking their intermediate filament networks. However, the relationship between alterations in cell adhesiveness and desmosomes is not well understood [2], and a direct correlation between the status of the desmosome and the transformed epithelial phenotype has not yet been established [6]. For example, reduction of desmosomes has been described in some carcinomas [2, 5, 7] and the magnitude of desmosomal reduction [8] or loss of desmosomal integrity [6] was correlated to the degree of transformation among cell lines with varying tumorigenic potential. Other studies have failed to show significant differences in the desmosomes of normal tissue, their tumors, and metastases [3, 9, 10]. Additionally, although cells contact and adhere prior to gap junction formation [11] few studies have focused on potential relationships between gap junctions (membrane channels which provide a direct pathway for the diffusion of small molecules (M_r < 1000 Da) between adjacent cells [12]), and desmosome junctions.

In this study, relationships between the degree of transformation, desmosome-mediated adhesiveness, and diffusion through gap junctions (one measure of gap junctional intercellular communication (GJIC)), were evaluated for a previously developed *in vitro* rat ovarian cell transformation sequence [13]. A computational method was developed (see Appendix) for quantitative comparisons of GJIC using fluorescence recovery after photobleaching (gap FRAP) data. This method al-

[1] This work was supported by NIH Grants HD26182 (R.C.B.) and DK07318 (L.S.S.) and a grant from the Texas Agricultural Experiment Station (R.C.B.).

[2] To whom correspondence and reprint requests should be addressed at Department of Pediatrics, M-609A, University of California at San Diego, 9500 Gilman Drive, La Jolla, CA 92093, Fax: 619-534-5497.

0014-4827/93 $5.00

lows for a comparison of systems with different recovery equilibria after photobleaching and its relationship to other methods of analyzing gap FRAP and FRAP data are discussed. Collectively the results identified a correlation between desmosomal losses and progression towards a metastatic phenotype. They suggested that quantitatively similar reduced levels of GJIC accompanied various conditions associated with reduced intercellular adhesiveness in the transformation sequence.

MATERIALS AND METHODS

Materials. Culture media, serum, and all general chemical reagents were purchased from Sigma Chemical Co. (St. Louis, MO). Tissue culture flasks and dishes were obtained from Corning Inc. (Oneonta, NY). Lab Tek slides and LUX permanox dishes were obtained from Nunc (Naperville, IL). Bacto-agar was purchased from Lakewood Biochemicals (Irving, TX). Cytodex microcarrier beads were purchased from Pharmacia (Piscataway, NJ). 5-Carboxyfluorescein diacetate (M_r 460) was purchased from Molecular Probes, Inc. (Eugene, OR). Gel electrophoresis and Western blot reagents including a goat anti-mouse gold conjugate were obtained from Bio-Rad Laboratories (Richmond, CA). A broad-spectrum cytokeratin monoclonal antibody (8.13) and a desmosomal-associated cytokeratin antibody (DK80) which reacts specifically with cytokeratin 8 were both obtained from Sigma. Monoclonal antibody to desmoplakin I and II was purchased from Biodesign International (Kennebunkport, ME) and monoclonal antibodies to desmoglein and tubulin were purchased from Oncogene Science (Uniondale, NY). A secondary biotinylated anti-mouse antibody and Texas red strepavidin were obtained from Amersham (Arlington Heights, IL).

Cell culture. The sequentially derived rat ovarian cell lines (SIGC, SV-SIGC, and T-SV-SIGC) [13] were maintained in DME supplemented with 5% fetal calf serum and corresponding passages were analyzed in parallel. Population doubling times were measured for each cell line from triplicate cultures plated at low density (100,000 cells in 25-cm^2 flasks) according to standard methods. The clonogenic potential of cell lines was compared in soft agar by counting colonies (greater than 40 cells) 14 days after seeding.

Calcium-switch studies [14] were conducted by washing subconfluent monolayers growing in standard media (SM) (calcium concentration = 1.2 m*M*) several times with calcium-magnesium-free PBS and replacing SM with low calcium media (LCM) (calcium concentration = 0.02 m*M*); the reversibility of the LCM effects was verified by subjecting cultures to the following sequence, SM→LCM→SM.

Indirect immunofluorescence and ultrastructural analysis. Subconfluent monolayers growing on Lab-Tek chamber slides were rinsed in 20 m*M* PBS, pH 7.2, fixed with 100% methanol at 20°C for 3 min, and rinsed quickly three times in acetone at −20°C. Slides were air dried and processed as described previously [13]. For ultrastructural analysis, subconfluent monolayers growing on Lux permanox dishes and tumor tissue were fixed in 3% glutaraldehyde, 2% paraformaldehyde in 0.067 *M* Sorenson's buffer at pH 7.3 for 2 and 12 h, respectively, and processed as described [13]. Two separate blocks from each cell line and from each of six SV-SIGC nude mouse tumors (three male, three female) were used for morphometric analysis. A minimum of six sections from each block were photographed at a magnification of ×3500. Desmosomes were counted on each photomicrograph and quantities expressed per 1000 μm of closely apposed membrane (within 50 μm).

In vitro migration assays. For the microcarrier bead assay, a stock bead suspension (25 mg bead/ml in serum-free DME) of Cytodex 3 beads was added to cell cultures which had been plated 24 h earlier and contained small colonies [15]. Bead cultures were incubated for 1–3 days allowing cells to attach to beads and undergo one to three doublings. Monolayer-covered beads were subsequently collected after tapping the sides of the flasks to free beads from the underlying monolayer. The beads were then washed three times and allowed to sediment at unit gravity, and the supernatant was removed to eliminate any suspended cells. The beads were resuspended in culture media, and added to fresh 35-mm culture dishes at a low density (approximately 100 beads per culture dish). For the wounding assay, subconfluent monolayers were obtained after 48 h of culture in 35-mm culture dishes and media was replaced with either fresh SM or LCM. Uniform cell-free linear areas of substratum ("wounds") [16] were produced by scraping monolayers with a 1- to 100-μl Eppendorf pipet tip while using a sterile glass slide, held parallel to the monolayer, as a straight edge. Cultures were photographed using phase microscopy as cells migrated off the beads onto the surfaces of the culture dishes or into the wounds.

Western blot analysis. For extraction of total cellular proteins, lysis buffer, consisting of 0.125 *M* Tris-Cl (pH 6.8), 4% SDS, 20% glycerol, 10% 2-mercaptoethanol, and 0.2 m*M* PMSF, was added directly to subconfluent monolayers (which had been rinsed three times with PBS) and lysed cells were scraped with a rubber policeman. Cytoskeletal extracts were prepared by adding lysis buffer consisting of PBS with 0.6 *M* KCl, 1.0% Triton X-100, 10 m*M* $MgCl_2$, 1.0 m*M* *p*-tosyl-L-arginine, and 1.0 m*M* PMSF [14] directly to culture dishes as above. After scraping, lysed cells were aspirated several times through a narrow pipet to enhance degradation. DNase I was added to a final concentration of 0.5 mg/ml and the mixture incubated for 5 min at 4°C. Proteins were separated by 10% SDS–PAGE, transferred to 0.20-μm nitrocellulose filters, probed with antibodies, and visualized with a goat anti-mouse gold conjugate followed by silver enhancement. Resulting bands were quantified by reflective scanning densitometry.

Assay of functional GJIC. GJIC was monitored by dye coupling with a Meridian ACAS 570 workstation (Meridian Instruments. Okemos, MI) using a fluorescence recovery after photobleaching (gap FRAP) technique [17]. Cells were plated in 35-mm culture dishes 36–48 h prior to analysis, stained with 10 μg/ml 5-carboxyfluorescein diacetate, and scanned as described [13, 18]. Briefly, a microscopic field containing abutting cells was selected for analysis and the inverted epifluorescence microscope objective focused an argon laser beam (488 nm) to a 1-μm-diameter spot. A series of point bleaches reduced dye photochemically in selected cells to a level sufficient for observation of fluorescence recovery without causing visible cell damage at the light microscopic level. Single cells without contacting partners did not recover fluorescence when photobleached (negative controls). Likewise, cells which were not point bleached did not lose significant amounts of fluorescence over short scanning periods (positive controls). After bleaching, redistribution of fluorescence in abutting cells was measured from sequential scans, beginning immediately postbleach and then at timed intervals.

The ACAS workstation software provided PR(t), the percent recovery at time t: $PR(t) = [[I(t) - I(0)]/I(-)] \times 100$, where $I(-)$, $I(0)$, $I(t)$ were the measured fluorescence intensities of the cell before (prebleach), at the first (immediate) postbleach scan, and at time t following the first scan, respectively. Programs were written in Matlab (Mathworks Inc., South Natick, MA) for data analysis. The fluorescence recovery data were expressed as the average ± SEM of the percentage of the prebleach value [19]. The mean fluorescence intensity level at the time of the first postbleach scan, I(0), was 28.7 ± 4% of the prebleach level, $I(-)$. This level was obtained by averaging the levels of all cells used in this study. The PR(t) curve was fit to a two-parameter equation to model the fluorescence recovery, $PR(t) = a(1 - e^{-kt})$, where the limiting value of the PR(t) curve is $a = 100 \times [IE - I(0)]/I(-)$ with IE defined as the equilibrium intensity (Eq. (A3) in the Appendix and [18]). The equilibrium term, a, and the rate constant, k, were estimated using a least squares fit of the data to this diffusion model, the covariance matrix of a and k was calculated, and

a goodness-of-fit test of the data to the model was performed. GJIC in the various cell systems was distinguished by their instantaneous rates of recovery, $I'(0)/I(0)$, at the time of the first postbleach scans (see Appendix for justification of this quantity as a measure of GJIC from gap FRAP data). These quantities were estimated by first estimating a and k as above, and then applying Eq. (A10) which expresses $I'(0)/I(0)$ in terms of a, k, and the fraction of laser bleaching at the time of the first postbleach scan (expressed as a percentage of the prebleach fluorescence intensity).

RESULTS

Progression toward in Vitro Metastasis Was Associated with a Stepwise Loss of Desmosomes and Cytokeratin

Tumor progression in the cell lineage was assessed by a cell scattering migration assay, which draws an analogy between tumor foci *in vivo* and monolayer-covered microcarrier beads in culture [15]. Since metastasis is a process whereby tumor cells leave their original location [1], an acquired ability of cells to detach from a monolayer in cell scattering assays is considered to be a step toward *in vitro* metastasis and thus assumed to represent reduced strength of adhesion between cells [20]. In SIGC (a spontaneously immortalized but not tumorigenic rat ovarian cell line) and SV-SIGC (a pSV3-neo clonal derivative), cells remained linked together and moved off of the beads as epithelial sheets onto the surfaces of the culture dishes (Figs. 1a and 1b). In contrast, T-SV-SIGC (a nude mouse SV-SIGC-tumor derivative) migrated away from the beads as individual fibroblastoid cells (Fig. 1c). This cell scattering assay was adapted from a wounding assay and parallel experiments verified that after wounding subconfluent monolayers, each cell type migrated into cell-free areas (wounds) with a pattern identical to that seen in corresponding bead experiments (data shown for SIGC, see results of calcium-switch experiments in the next section).

Other features consistent with tumor progression included a reduction of the population doubling time, from 24 h in SIGC to 18 h in both SV-SIGC and T-SV-SIGC, and an increase in soft agar cloning efficiency, from 0% in SIGC to 1% in SV-SIGC and to greater than 80% in T-SV-SIGC. In the soft agar assays there were sparsely scattered colonies of 3 to 10 cells in SIGC (which did not appear to increase in size during 4 weeks of culture) compared to SV-SIGC which formed relatively small dense colonies consisting of up to 60 cells and T-SV-SIGC where there were larger stellate colonies consisting of up to several hundred cells each (Fig. 1).

Desmosomes were evaluated by immunochemical and complementary ultrastructural techniques. A panel of monoclonal antibodies consisted of antibodies to desmoplakin I and II (the major desmosomal proteins), to desmoglein (an adhesive glycoprotein of desmosomes), to cytokeratin 8 (a desmosomal-associated cytokeratin), as well as to a broad-spectrum cytokeratin antibody. Antibodies to desmoplakin I and II (Figs. 1g–1i) and cytokeratin 8 (Figs 1j–1l) demonstrated a nearly continuous, punctate label in areas of cell–cell association in SIGC. Label was reduced in SV-SIGC and essentially absent in T-SV-SIGC, where the only staining observed was perinuclear (Fig. 1l). Antibodies to desmoglein (see results of calcium-switch experiments below) and a broad spectrum of cytokeratins (Figs. 1m–1o) also exhibited a stepwise loss of label associated with sequential transformation.

A sequential attenuation of the desmosome-intermediate filament complex was apparent in electron micrographs, which also suggested that both perinuclear and desmosomal-associated filaments were absent in the nude mouse SV-SIGC tumors (Fig. 2). The desmosomes were quantified by ultrastructural morphometry and expressed per 1000 μm of closely apposed membrane (within 50 μm) in the sequence, 68.5 (SIGC), 44.5 (SV-SIGC), 23.1 (female SV-SIGC tumors), 20.7 (male SV-SIGC tumors), and 2.5 (T-SV-SIGC). These results suggested that about a third of the desmosomes were lost from SIGC → SV-SIGC and nearly all of the rest were lost from SV-SIGC → T-SV-SIGC. A complementary Western blot analysis of whole cell extracts (Fig. 3), by reflective scanning densitometry of triplicate blots, suggested that relative to SIGC the quantity of desmosomal-associated cytokeratin 8 in SV-SIGC was 76% (SD ± 7%, $P \leq 0.001$), and nearly zero in T-SV-SIGC (where it was 0.03% in one blot and below the detection limit of the densitometer in the other two).

Collectively, the results illustrated that SIGC → T-SV-SIGC was associated with both a change from movement of cells as an epithelial sheet to detachment of individual cells that assumed a fibroblastoid morphology during migration (compare SIGC (Fig. 1a) and T-SV-SIGC (Fig. 1c)) and the loss of the desmosome-cytokeratin intermediate filament complex (compare SIGC (Figs. 1g, 1j, and 1m; 2a; 3, top blot, lanes 1 and 2) and T-SV-SIGC (Figs. 1i, 1l, and 1o; 2b; 3, top blot, lanes 5 and 6)).

Manipulation of Extracellular Calcium Levels in SIGC Cultures Reversibly Induced a Phenotype Reminiscent of T-SV-SIGC

Interactions between adhesiveness and cell movement in SIGC were evaluated using a calcium-switch system whereby desmosomes are reversibly internalized following a switch from SM to LCM [14]. Following a switch from SM to LCM, a loss of staining of desmosomal-associated components in SIGC was evident at the first postswitch (1 h) time point, and by 4 h specific staining was essentially absent at cell–cell boundaries (Fig. 4). Although the results are shown for desmoglein staining, similar results were seen using desmoplakin

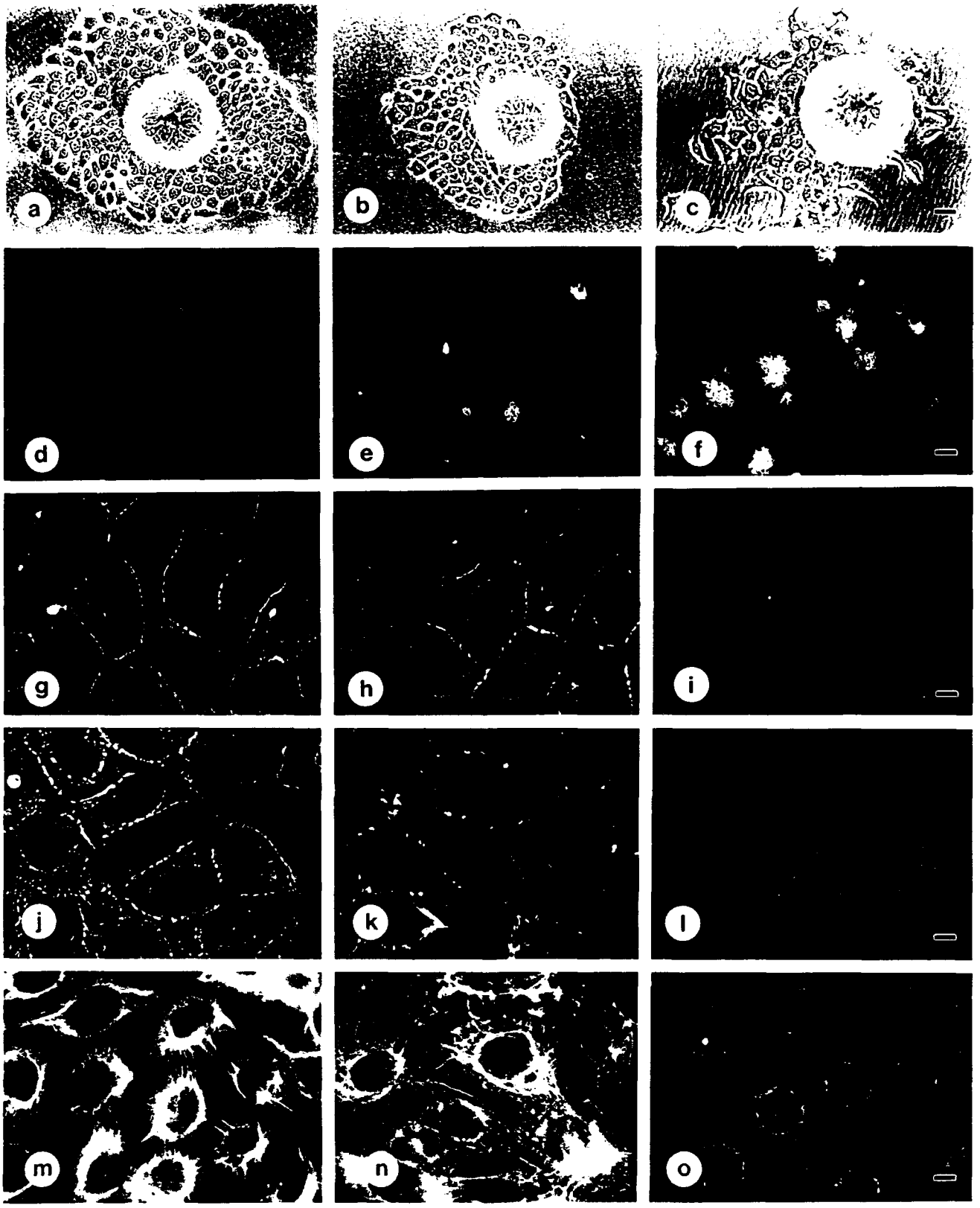

FIG. 1. Alterations in cell movement, growth, desmosomes, and cytokeratins in the transformation sequence, SIGC (column 1) → SV-SIGC (column 2) → T-SV-SIGC (column 3). Phase-contrast microscopy of monolayers moving off of spherical microcarrier beads onto the

and cytokeratin 8 antibodies (refer to Figs. 4a, 1g, and 1j for a comparison of desmoglein, desmoplakin, and cytokeratin 8 antibody staining patterns in SM). After 6 h in LCM, reversibility of the low calcium effects was verified by switching cultures back to SM where defined staining at the majority of cell–cell boundaries was clearly evident after 4 h recovery in SM (Fig. 4c).

In a wounding assay, SIGC in SM remained linked together as they migrated into the wounds which was similar to that seen as they migrated off of microcarrier beads onto the surface of the culture dish (compare Figs. 4d and 1a). However, in cultures switched to LCM prior to wounding, individual and small groups of cells were observed within the wounds (Fig. 4e), and a fibroblastoid morphology reminiscent of that seen in T-SV-SIGC cells as they migrated off of microcarrier beads was present (compare Figs. 4e and 1c). Reversibility of the effects of LCM on migration was verified by a sequence of calcium switching and wounding (Fig. 4f). A composite result showed that both SIGC (SM → LCM) and SIGC → T-SV-SIGC resulted in the acquired ability of cells to detach from a population during migration (compare Figs. 1a and 4d with Figs. 1c and 4e) and an associated loss of desmosomal components at areas of cell–cell contact (compare Figs. 1g and 1j; 4a with Figs. 1i and 1l; 4b).

Different Cellular Conditions Associated with Reduced Adhesiveness Correlated with Similar Levels of GJIC

Effects of LCM on Preexisting GJIC. Relationships between GJIC and calcium-dependent adhesiveness were evaluated by dye coupling using gap FRAP. Gap FRAP data collected 1 min after the first postbleach scans identified a gradual reduction in dye coupling over the first 12 h after switching SIGC from SM to LCM, with no further losses observed over the next 12 h (Fig. 5). Among cell lines in the lineage, there was a sequential reduction of dye coupling associated with sequential steps in the transformation process during standard conditions (standard conditions refers to cells in SM and interphase and are assumed unless otherwise noted) which was consistent with that previously described [13] (Fig 6). Time-course evaluations revealed that LCM also reduced dye transfer in SV-SIGC but not significantly in T-SV-SIGC (Fig. 6). LCM results in Fig. 6 and henceforth, unless otherwise noted, refer to those obtained after 12 h in LCM since additional reductions were not observed after this time point. Reversibility of the effects of LCM on measured dye transfer in SV-SIGC was verified 12 h after switching cultures from LCM back to SM.

A quantitative analysis of gap FRAP data in the SIGC lineage. Previously gap FRAP data was used to analyze GJIC by comparing the rate, k, at which different systems approached fluorescence recovery equilibrium after photobleaching; higher k values were assumed to indicate greater GJIC [18, 21, 22]. Ratios of k are suitable measures of diffusion either for systems which recover fluorescence to the same equilibrium level, a (Appendix, Eq. (A11) [18]), or for which there is insignificant loss of mobile fluorophores during the recovery phase (see Appendix and [23]). In this study, the estimated parameters of both a and k for many of the cell systems differed. For example, over the first minute SIGC recovered over three times the amount of fluorescence recovered by T-SV-SIGC (Fig. 6) yet the estimated k values for these systems were similar, $0.531 \pm 0.070\ \text{min}^{-1}$ and $0.595 \pm 0.221\ \text{min}^{-1}$, respectively (Fig. 7). Thus based on recovery over 1 min, the GJIC would be quite different for the two system, but based on estimates of k, the GJIC would be similar.

Equation (A8) was used to compare the diffusion coefficients of the various cell systems. It was derived from Eq. (A4) of the Appendix which is an interpretation of Fick's first law of diffusion. Equation (A8) expresses the ratio of the diffusion coefficients in terms of the ratio of the instantaneous rates of recovery at the time of the first postbleach scan, $I'(0)/I(0)$. To estimate $I'(0)/I(0)$, the recovery data was fit to Eq. (A3) $\text{PR}(t) = 100xa(1 - e^{-kt})$, and $I'(0)/I(0)$ was calculated using Eq. (A10), $(I'(0)/I(0) = a \cdot k \cdot I(-)/I(0))$. χ^2 values measuring the fit of the various data sets to the theoretical curves were calculated from the data and the significance levels were obtained from tables of the χ^2 distribution with two degrees of freedom (the significance level is the probability of a higher χ^2 error assuming that the model is correct). The mean level of significance for all data described in this report was 90% and the values ranged from 75–99%, indicating that the two-parameter model fit the gap FRAP data with high χ^2 levels of significance. Error analysis [18] revealed a strong negative correlation ($\geq$90%) between the parameters a and k, and thus the standard deviation (SD) of ak, as depicted in the error bars in Fig. 8, is significantly less than would be the case if a and k were independent [24].

surfaces of the culture dishes (photographed after 60 h in culture), SIGC (a), SV-SIGC (b), T-SV-SIGC (c). As explained under Materials and Methods, microcarrier beads were coated with monolayers prior to their inoculation into culture dishes. Dark-field microscopy of cell lines in soft agar 14 days after seeding single suspensions of 25,000 cells in each 60-mm^2 culture dish, SIGC (d), SV-SIGC (e), T-SV-SIGC (f). Identification of desmosomes by indirect immunofluorescence microscopy using monoclonal antibodies to desmoplakins (g–i) and cytokeratin 8 (j–l), both antibodies identified bright punctate staining at cell–cell boundaries in SIGC (g, j), which was reduced in amount but not in intensity in SV-SIGC (h, k) and was essentially absent in T-SV-SIGC (i, l). A broad-spectrum cytokeratin antibody identified both intense fibrillar cytoplasmic and perinuclear staining of cytokeratins in SIGC (m) which was slightly reduced in SV-SIGC (n) but only attenuated punctate perinuclear staining in T-SV-SIGC (o). Bars: (a–c) 20 μm; (d–f) 100 μm; (g–o) 5 μm.

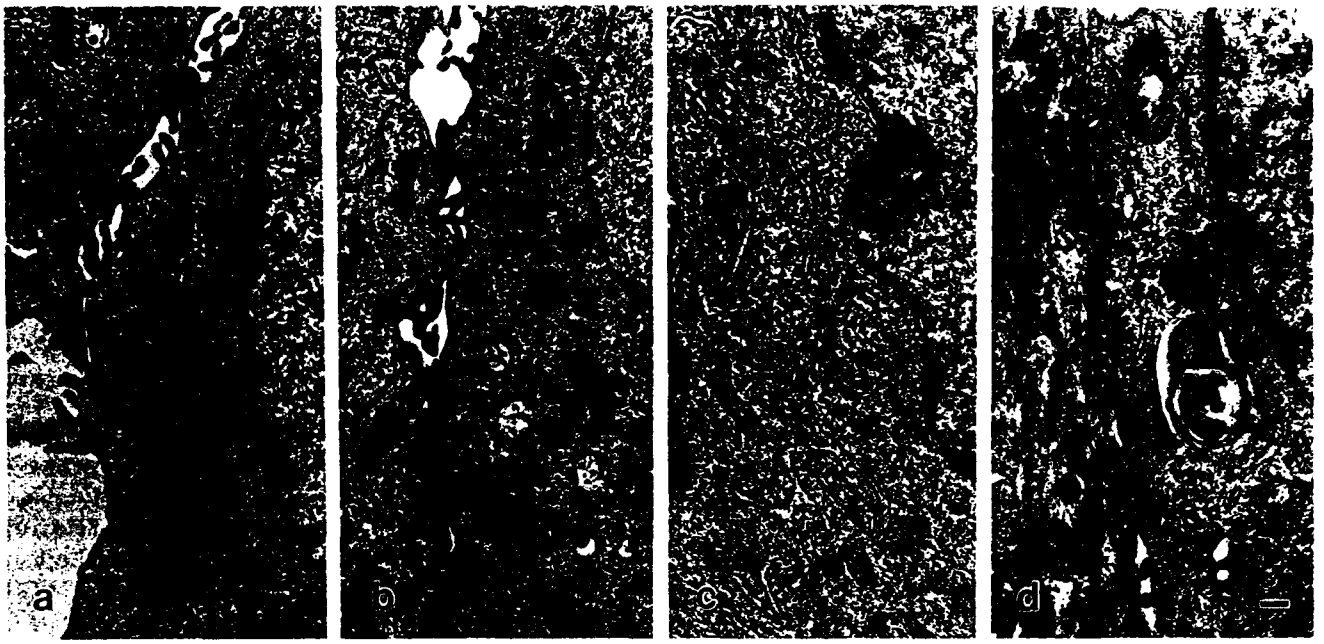

FIG. 2. A comparison of the ultrastructural features of the desmosome–intermediate filament complex in the transformation sequence and *in vivo*. Portions of closely apposed cells are shown and a nucleus is seen in the cell to the right of each cell pair. In SIGC (a) continuity was seen between desmosomal-associated and perinuclear filaments (cell at right) which extended to the adjacent cell membrane at the desmosome plaques (cell at left). In SV-SIGC (b) both desmosomal-associated and perinuclear filaments were seen, but the continuity between them as well as the apparent transmembrane continuity observed in SIGC appeared disrupted. In the SV-SIGC nude mouse tumor (c) and in T-SV-SIGC (d) perinuclear filaments were not observed and desmosome plaques appeared in the absence of associated filaments. Bar, 100 nm.

$I'(0)/I(0)$ for the various cell systems was calculated as described above (using data measured every 1 min for 4 min). As can be seen in Fig. 8, there was a stepwise reduction of $I'(0)/I(0)$ ($P \leq 0.05$) as SIGC was transformed (SIGC → SV-SIGC → T-SV-SIGC). Compared to their respective rates during standard conditions, both mitosis and LCM were associated with reduced rates in SIGC ($P \leq 0.05$) and SV-SIGC ($P \leq 0.05$) and slight, but not significant, reductions in T-SV-SIGC ($P \geq 0.05$). $I'(0)/I(0)$ for (i) all T-SV-SIGC systems, (ii) all LCM systems, and (iii) all mitosis systems were not significantly different ($P \geq 0.05$). Thus the magnitude of reduction of a given cell type, relative to their respective rates during standard conditions, varied but the reduced levels themselves did not.

Ratios of $I'(0)/I(0)$ are equal to ratios of the diffusion coefficients for respective systems and thus reductions in $I'(0)/I(0)$ correspond to reductions in the diffusion coefficient, D. As ratios of D are used to compare relative GJIC, a reduction in $I'(0)/I(0)$ corresponds to a reduction in GJIC. These estimates of $I'(0)/I(0)$ show that GJIC was reduced to similar levels under the following conditions: (i) transformation to T-SV-SIGC, (ii) mitosis, and (iii) LCM. Dose–response data indicated that SIGC cultures in 0.5 m*M* 1-octanol were similarly reduced. Octanol is a known gap junctional uncoupling agent [for review see 25]. This reduced level was distinguished from an uncoupled or "noise" level by comparison with SIGC in 1.0 m*M* 1-octanol for which there was no significant dye transfer (Figs. 8 and 9).

The values of $I'(0)/I(0)$ were grouped into four categories of GJIC and denoted as (i) high (SIGC), (ii) intermediate (SV-SIGC), (iii) reduced (T-SV-SIGC, all LCM and mitosis data, and SIGC + 0.5 m*M* octanol), and (iv) noise (SIGC + 1.0 m*M* octanol). The average of $I'(0)/I(0)$ for these categories were 76.4, 37.3, 19.3, and 4.2 min^{-1}, respectively. Since ratios of D are equal to ratios of $I'(0)/I(0)$, relative diffusion for these systems were compared. Letting D_i denote the diffusion coefficient for category i, the parental SIGC cells (Category 1) recovered at 2 times the rate of the intermediate level (Category 2) (i.e., $D_1/D_2 = 2.0$), at 4 times the reduced level (Category 3) (i.e., $D_1/D_3 = 4.0$), and at 20 times the noise (1.0 m*M* 1-octanol) level (Category 4) (i.e., $D_1/D_4 = 20$).

The estimate of $I'(0)/I(0)$ was reproducible using different measurement schemes. $I'(0)/I(0)$ was estimated using SIGC data collected at different intervals and over different lengths of time. A comparison of the measured recovery data sets is illustrated by showing a curve which was fitted to the (1, 4, 80) set and by plotting measured data from the various sampling schemes relative to this "theoretical" recovery curve (Fig. 9). For example, a (1, 4, 80) sampling scheme denotes data col-

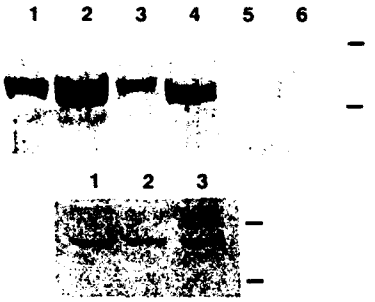

FIG. 3. Western blot analysis of relative amounts of desmosomal-associated cytokeratin in the SIGC lineage. Equal protein amounts of cytoskeletal (top blot, lanes 1, 3, and 5) or whole cell (top blot, lanes 2, 4, and 6 and all bottom blot lanes) extracts were separated by 10% SDS–PAGE, transferred to nitrocellulose, and probed with antibodies to cytokeratin (top blot) or tubulin (bottom blot). Bands were visualized with a goat anti-mouse gold conjugate followed by silver enhancement and quantified by reflective scanning densitometry. Top blot: SIGC (lanes 1 and 2), SV-SIGC (lanes 3 and 4), T-SV-SIGC (lanes 5 and 6). Bottom blot: SIGC, SV-SIGC, and T-SV-SIGC (lanes 1–3, respectively). M_r standards are at 50 and 75 kDa. Cytokeratin 8 (M_r 52,500) was abundant in SIGC and SV-SIGC extracts. Lanes were overloaded with protein to illustrate the relatively low level of cytokeratin 8 in T-SV-SIGC which is only faintly visible. The amount of cytokeratin (using tubulin as an internal control) in SV-SIGC and T-SV-SIGC extracts was 75 and 0.03% of that in SIGC extracts, respectively, in this blot (top blot, lanes 4, 6, and 2).

lected at 1-min intervals over a period of 4 min from 80 recovering cells. Values are stated ± estimated standard deviations of the value. $I'(0)/I(0) = 76.4 \pm 5.7$ min^{-1}; $I'(0)/I(0)$ was 76.3 ± 9.7, $76.2 \pm 10.3\%$ min^{-1}, and $76.5 \pm 10.00\%$ min^{-1} for a (1, 4, 80) and three replicate (1, 4, 25) data sets, (1), (2), and (3), respectively. The estimates of $I'(0)/I(0)$ were calculated from estimates of the parameters (a, k) which were ($41.3 \pm 2.7\%$, 0.53 ± 0.07 min^{-1}), ($44.9 \pm 5.5\%$, 0.49 ± 0.12 min^{-1}), ($40.1 \pm 4.34\%$, 0.54 ± 0.13 min^{-1}), and ($38.8\% \pm 4.2\%$, 0.57 ± 0.13 min^{-1}) respectively. The significance levels of the χ^2 test were 82, 95, 90, and 90%, respectively. The minimum practical measurement interval for collecting fluorescence recovery data was 0.4 min and for (0.4, 9.6, 6), $I'(0)/I(0) = 81.9 \pm 6.9\%$ min^{-1}, (a,k) = ($41.3 \pm 1.6\%$, 0.53 ± 0.7 min^{-1}), and the significance level of the χ^2 test was greater than 99%.

Recovery for the short-term data sets was compared with long-term recovery using (5, 30, 4) sampling (sparse measurement intervals minimize fluorescence fading for data collected over extended time periods). Figure 9 shows that fluorescence reaches a peak and then decays although the model $PR(t) = 100 \times a(1 - e^{-kt})$ predicts a stable equilibrium. The analysis herein used the model (Eq. (A3)) to calculate $I'(0)/I(0)$ from Eq. (A10). To estimate the derivative at the time of the first postbleach scan ($I'(0)$) a good fit in the early recovery period between the measured and modeled data is required. Sparse sampling, e.g., (5, 30), may not provide an adequate fit.

DISCUSSION

An analysis of the rat ovarian cell lineage SIGC, during tumor progression and manipulation of calcium-dependent adhesiveness, suggested that changes in desmosomes, adhesiveness, and GJIC occurred as coordinated processes. Increased growth in soft agar and a cell scattering assay provided evidence of sequential progression toward *in vitro* metastasis. In the cell scattering assay, the progression of SIGC, which moved off of microcarrier beads as epithelial sheets, to T-SV-SIGC, which migrated away from microcarrier beads as individual fibroblastoid cells, was reminiscent of epithelial–mesenchyme transitions (EMT) [26]. EMT occurs during embryogenesis when epithelial cells dissociate and migrate as individual cells and is associated with a reduction or loss of epithelial characteristics including cytokeratins, desmosomes, and GJIC like that seen in the SIGC lineage. An induction of an EMT-like conversion in SIGC following a switch from SM to LCM was consistent with previous studies showing that when cultured in LCM, rat bladder cell lines of low tumorigenic potential [6] and normal keratinocytes [27] resembled their transformed counterparts. Epithelial to fibroblastoid conversions between cell lines, from a variety of transformation systems, have led to a hypothesis that there may be common cellular mechanisms which participate in changes characteristic of both morphogenetic EMT and malignant EMT-like conversions [6, 16, 29].

The "desmosome" junctions in the nude mouse SV-SIGC tumors and in T-SV-SIGC appeared similar to the primitive desmosome and desmosome-like residual junctions previously reported in human ovarian tumors [28]. They were devoid of desmosomal-associated components such as cytokeratins and in contrast to the desmosome–intermediate filament complexes observed in corresponding normal ovarian tissue and in SIGC. Separation of cells from a primary ovarian tumor *in vivo* may itself be a critical step in ovarian carcinogenesis since detached ovarian cells are potentially free to implant on any peritoneal surface without having to translocate across any additional biologic barriers [30, 31]. However, the mechanism of separation is elusive, in part, because over 75% of ovarian neoplasms first present at an advanced stage with cancer cells already scattered throughout the abdominal cavity [30, 31]. Further studies may reveal if EMT-like transitions from SIGC →→ T-SV-SIGC or following a switch from SM to LCM constitute *in vitro* reflections of mechanisms by which ovarian cells escape from primary tumors.

A reduction of both desmosomes and GJIC in the lineage was consistent with previous observations of a stepwise reduction of desmosomes and gap junctions in sequential transformation stages, normal → nonmalignant pathological → preinvasive → invasive, of human

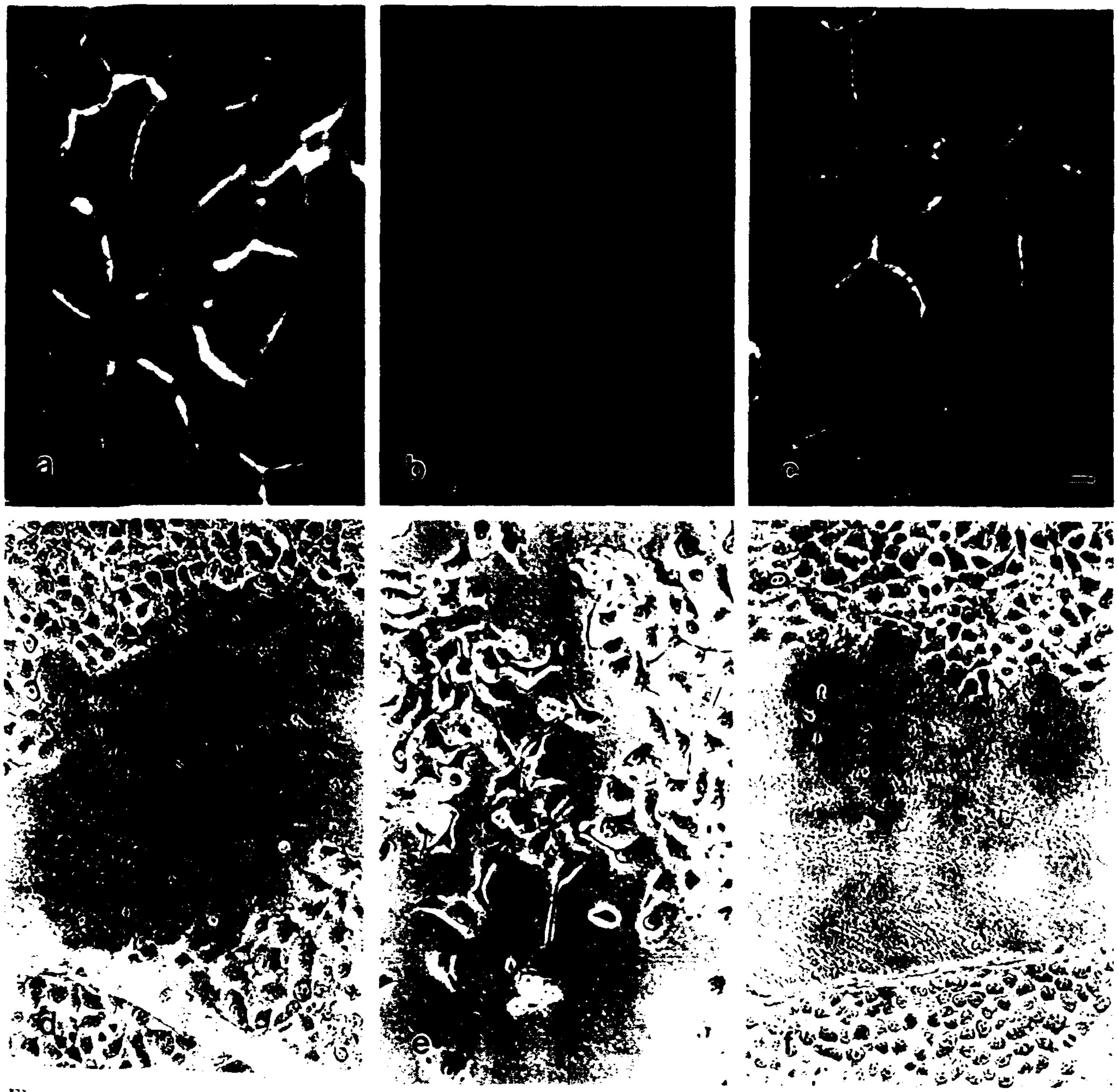

FIG. A reversible loss of desmosomes ... fluore... of SIGC using antibody to desmoglein ... nge in movement pattern in SIGC ... witch system. (a ... immuno... (d-f) Phase-contrast microscopy of ... monolayer ... ltured in SM for 48 h (a), ... to LCM for 4 h (b), and ... k to ... for 4 h (c). Cells were cultured in SM for 48 h, and ... edia was replaced ... wounding as cells mo... into cell-free areas (w... in the culture dishes. a pipet tip to produce a wound. In S...), cel... esh SM (d) ... LCM (e) immediately prior to scraping monolayers with epithelial sheets of cells were observed ... the w... ined linked tog... ...oved as an epithelial sheet. In LCM (e), cells detached from ... tern was seen after return to SM, i.e., SM ... th a ... blastoid ... rphology. (f) A characteristic SIGC epithel... pattern of movement ... ch back to SM and allow 10 h recovery → w... → sw... h to LCM ... wound monolayer, a... llow 10 h for cells ... migrate into wound → ... 20 μm. ...nol... er again ... nd allow 10 h to m... ...to wound → photograph. Bars: (a–c) 5 μm;

ce... epithelium [5], and fewer gap ju... ...ns ... desmoso... n highly, compared to weakly, ... astatic clones isola... from rat mammary carcinoma ... lines [8]. This study extended previous results by co... ...ing de... nosome a... GJIC losses during clonal evolution of a trai... sformed ... enotype, SIGC →→ T-SV-SIGC. Additionally, th... ...sults complemented previous studies investigatin... e interplay between the cadherins (a fam-

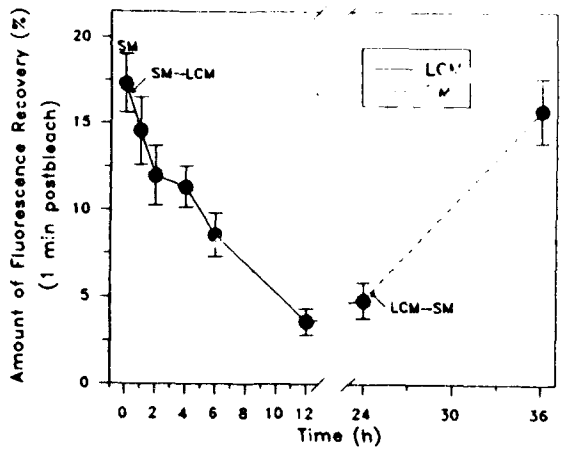

FIG. 5. One-minute fluorescence recovery amounts after photobleaching in SIGC as a function of time in a calcium-switch system. One-minute recovery amounts were measured in cells cultured in SM, over a 24-h period after switching from SM to LCM, and following a 12-h recovery after switching from LCM back to SM. The vertical axis is PR(1) which is $100 \times (I(t) - I(0))/I(-)$ where t is minutes after the first postbleach scan, $I(t)$ is the intensity at time t, $I(0)$ is the intensity at the time of the first postbleach scan, and I(-) is the prebleach intensity. Error bars represent the SEM of the mean percentage recovery.

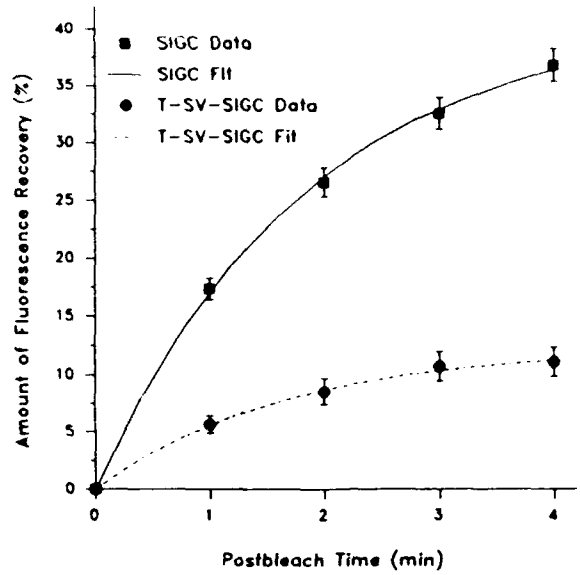

FIG. 7. A comparison of measured and theoretical fluorescence recovery in SIGC and T-SV-SIGC. The measured data were obtained by sampling data every 1 min for 4 min, denoted as a (1, 4) sampling scheme. The parameters were estimated by fitting the data to Eq. (A3). The estimated values and standard deviations of a were 41.3 ± 2.8% and 12.4 ± 1.7% and for k were 0.531 ± 0.070 min^{-1} and 0.595 ± 0.221 min^{-1} for SIGC and T-SV-SIGC, respectively. For each data set, Eq. (A3) is plotted. χ^2 significance levels were 83 and 95% for SIGC and T-SV-SIGC, respectively. Using the estimated values of the parameters, the instantaneous rates of recovery at the time of the first postbleach scan, $I'(0)/I(0)$, were calculated using Eq. (A10) with $I(-)/I(0) = 0.0348$. $I(-)/I(0)$ is the reciprocal of the fraction of initial laser bleaching which averaged 28.7% of the prebleach level as described under Materials and Methods. Values of $I'(0)/I(0) \times 100\%$ ± min^{-1} standard deviations were 76.4 ± 5.7% min^{-1} and 25.9 ± 5.5% min^{-1} for SIGC and T-SV-SIGC, respectively.

ily of calcium-dependent cell–cell adhesion molecules) [for review see 32], functional adhesiveness, and GJIC [33, 34] by identifying similar interactions between desmosomes, adhesiveness, and GJIC.

GJIC was categorized according to ratios of the proportionality constants, D, in Fick's first law of diffusion as estimated using Eq. (A8). Both transformation to T-SV-SIGC and a switch to LCM apparently reduced the diffusion coefficient D of SIGC to similar levels. Specifically, the magnitude of reduction in SIGC following a switch to LCM was similar to that seen following SIGC →→ T-SV-SIGC or from Category 1 to 3. Consequently, since the rate during standard conditions in SV-SIGC (Category 2) was less than that of SIGC (Category 3), the absolute magnitude of its reduction in LCM, from Category 2 to 3, was also less. Since the rate of GJIC in T-SV-SIGC (Category 3) did not change categories in LCM, these results suggested that T-SV-SIGC probably did not have significant calcium-dependent cell–cell adhesion. Additionally, a comparison of the reduced (Category 3) LCM and T-SV-SIGC rates to the rates established during mitosis is of potential biological significance since mitosis is considered to be the lowest point of adhesiveness between cells in the cell cycle [35] and all mitotic cell systems fell into Category 3 rates. Since Category 3 diffusion rates were significantly higher than a noise rate (Category 4) defined by the presence of 1.0 mM 1-octanol in SIGC cultures, Category 3 rates likely represented actual metabolic cou-

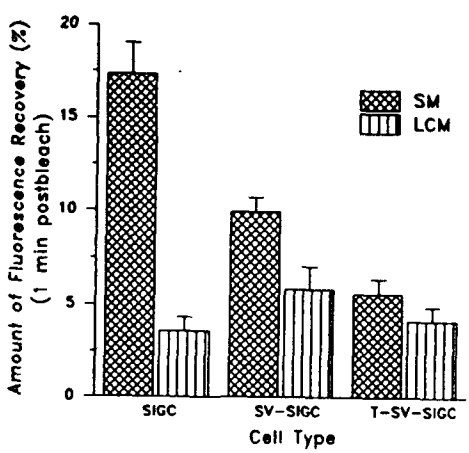

FIG. 6. A comparison of the 1-min fluorescence recovery amounts in the SIGC lineage in SM and LCM. One-minute recovery amounts were measured for SIGC, SV-SIGC, and T-SV-SIGC in SM and 12 h after switching from SM to LCM. The vertical axis is PR(1) as defined in the legend to Fig. 5. Error bars represent the SEM of the mean percentage recovery.

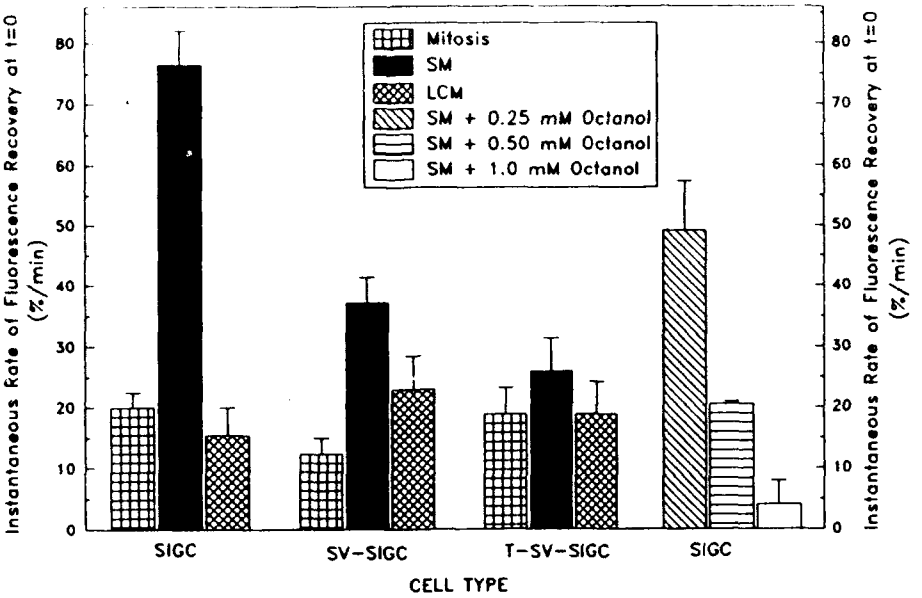

FIG. 8. Comparison between all cell systems of the estimated instantaneous rates of recovery at the time of the first postbleach scan, $I'(0)/I(0)$, from (1, 4) sampling. Unless otherwise noted, all cells were cultured in SM and scanned during interphase. The notation SM refers to cell systems in standard conditions, i.e., SM in interphase. LCM, mitosis, and octanol systems were scanned 12 h after switching from SM to LCM, during the metaphase plate stage and immediately after the addition of octanol, respectively. Error bars represent the standard deviation (SD) of the estimate, $I'(0)/(I(0)$. The vertical axis is $100 \times I'(0)/I(0)$ where $I(0)$ is the intensity of fluorescence at the $t = 0$ and I' is the derivative of I.

pling. Further, these results suggested that the levels of diffusion characteristic of Category 3 were not necessarily contingent on calcium-dependent adhesion. Future studies may reveal if GJIC during various cellular states in other cell systems also fall into similar distinct categories of diffusion.

The estimates of GJIC were obtained using the technique developed in the Appendix. The technique is discussed here within the context of previous techniques used to analyze gap FRAP and FRAP data: There are two common techniques for analyzing gap FRAP data, i.e., (i) calculating the average rate of fluorescence recovery over a specific time interval [e.g., 13, 19, 22, 36–38] and (ii) using Fick's first law of diffusion to model fluorescence recovery [18, 21, 22]. Initially Fick's law was applied assuming that the bleached cell would recover to its prebleach level [21]. The rate of recovery was obtained by fitting the data to a one parameter equation and the diffusion coefficient was calculated from this rate constant. However, collectively results from gap FRAP studies suggest that there may not be 100% recovery (to the prebleach level) [e.g., 13, 18, 19, 21, 22, 36–38] and the results presented in this study indicated that different cell systems may recover to different fluorescence levels.

Peters [23] modeled FRAP data using a form of Fick's law that allows for partial recovery. In this model, it was assumed that there is a certain fraction of immobile fluorophores which remains essentially constant over the recovery interval and the recovery curve is modeled using a two-parameter equation. The rate parameter is related to the diffusion coefficient and the other parameter can be solved for the fraction of immobile fluorophores. This approach has also been used to study gap FRAP [18]. This approach was initially used to analyze the gap FRAP data presented here but different recovery equilibria led to inconsistent results. For example, Fig. 7 showed that the estimated rate constants for T-SV-SIGC and SIGC were similar, yet Fig. 6 shows that SIGC recovered much more rapidly. This could indicate that diffusion coefficients were similar in the two systems and that the concentration of immobile fluorophores is much higher in the T-SV-SIGC cells than in the SIGC cells.

However, ultrastructural results suggested that the amount of gap junctional membrane in T-SV-SIGC is considerably reduced compared to that in SIGC (Stein and Burghardt, unpublished observations) and another interpretation of the estimated parameters is suggested by the work of Zimmerman and Rose [39]. In their analysis of dye coupling using dye injection, they use a model that accounts for immobilization and loss of the fluorophores over the recovery period. Allowing for these possibilities in our analysis of gap FRAP led to Eq. (A8) which, under certain conditions, equates ratios of the diffusion coefficients in Fick's first law to ratios of the instantaneous rate of recovery at the time of the first postbleach scan. The model recovery Eq. (A3) is a com-

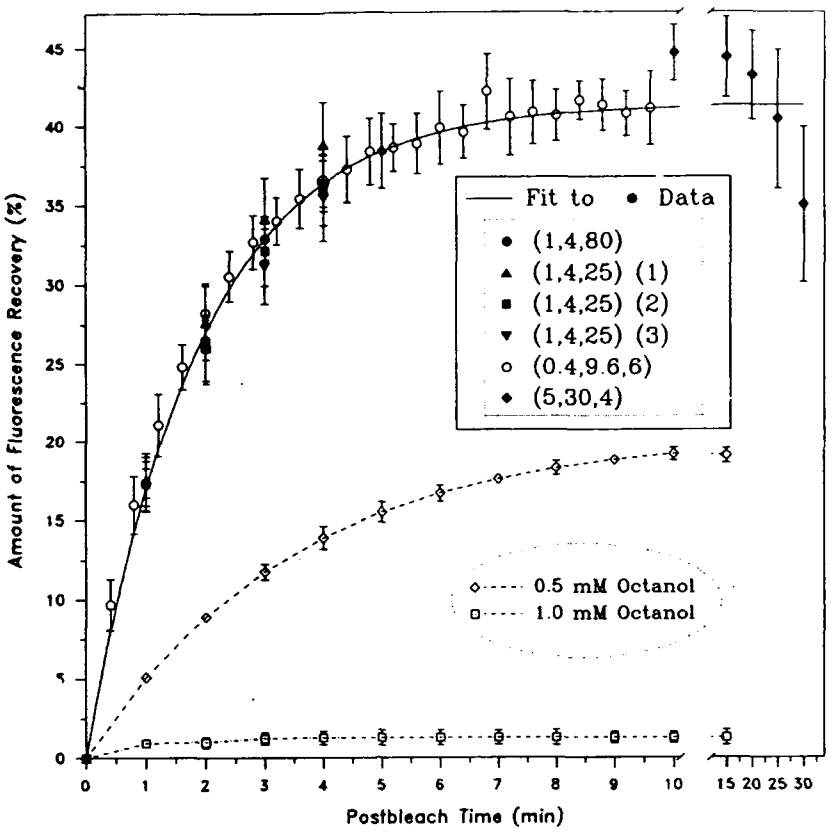

FIG. 9. A comparison of the measured percent recovery data in SIGC using alternate measuring schemes to a curve fitted to (1, 4, 80) data and to the effects of 1-octanol. As explained in the text (1, 4, 80) refers to measured fluorescence recovery data which was obtained at 1-min intervals over 4 min from 80 bleached cells. The theoretical curve was obtained by fitting the (1, 4, 80) data to the model percentage recovery curve (Eq. (A3)) and then plotting fitted (theoretical) data out to 30 min. The level of significance of the χ^2 goodness-of-fit test measured (1, 4, 80) data to this model curve was 82%. Measured data from three replicates of a (1, 4, 25) sampling scheme, a (0.4, 9.6, 6) and a (5, 30, 4) sampling scheme are shown relative to this curve. The χ^2 test was used to evaluate the fit between the (1, 4, 80) theoretical curve and the (0.4, 9.6, 6) data, and the significance level was greater than 99%. Significance levels were also calculated to evaluate the fit between the each of the (1, 4, 25) and (0.4, 9.6, 6) measured data sets and their respective theoretical recovery curves, and these values are reported in the text. The effects of 1-octanol in cultures are shown by plotting measured recovery curves. The vertical axis is PR(t) as defined in the legend to Fig. 5. Error bars represent the SEM of the mean percentage recovery of measured data.

putational device to calculate the instantaneous rate (Eq. (A10)). This method of calculating the derivative is validated by the close fit of the recovery data from the first 4 min to this model equation (Fig. 9). If the estimated recovery level for two systems is similar, then the ratio of the diffusion constants for these systems reduces to the ratio of the rate constants (Eq. (A12)) which has been used as a measure of relative diffusion [23].

In conclusion, the results support the utility of the SIGC lineage in defining *in vitro* basic relationships between different cell–cell contacts and suggest that relative values of the diffusion coefficient may be useful in categorizing the effects of many different processes on the gap junctions. An analysis of the possible differential effects of cellular factors (such as transformation and variations during the cell cycle) and of treatments (such as octanol) on the mobility of the fluorophores through the cytoplasm would be useful in verifying the theoretical foundations of gap FRAP, i.e., that gap junction permeation is the rate-limiting step in intercellular diffusion of dye, and further defining potential processes, in addition to gap junctions themselves, which may influence the rate of observed GJIC.

APPENDIX

Instantaneous Rate of Recovery of Fluorescence after Photobleaching (gap FRAP)

GJIC between cells was monitored by dye coupling with a Meridian ACAS 570 workstation (Meridian Instruments, Okemos, MI) using a fluorescence recovery after photobleaching (gap FRAP) technique, which is an extension of FRAP to gap junctions [17]. The ACAS

workstation software provided the percentage recovery at time t

$$\mathrm{PR}(t) = 100 \times \frac{I(t) - I(0)}{I(-)}, \tag{A1}$$

where $I(t)$ is the intensity at time t, $I(-)$ is the prebleach intensity, and $t = 0$ is the time of the first postbleach scan.

The recovery of fluorescence intensity in the bleached cell has been modeled by

$$\frac{\mathrm{IE} - I(t)}{\mathrm{IE} - I(0)} = e^{-kt}, \tag{A2}$$

where IE is the equilibrium intensity after recovery. Schindler *et al.* equate IE with the prebleach intensity [21]. Previous FRAP [23] and gap FRAP [13, 18, 19, 21, 22, 36–38] studies suggest that the equilibrium after photobleaching is below the prebleach level, and therefore, the recovery was modeled as

$$\mathrm{PR}(t) = 100 \times a(1 - e^{-kt}), \tag{A3}$$

where $a = (\mathrm{IE} - I(0))/I(-)$ [18, 23]. The constants a and k were estimated using a least squares fit of the data to Eq. (A3), the variance and covariance of a and k were estimated, and the χ^2 goodness of fit test was used to compare the model with the data [18].

These approaches to modeling the recovery data follow from Fick's first law of diffusion

$$F = -D \frac{\partial C}{\partial x},$$

where F is the rate of transfer per unit area of section, C is the concentration of the diffusing substance, x is the space coordinate measured normal to the section, and D is the diffusion coefficient [reviewed in 40]. For the system under study, a recovering cell attached to supply cells through gap junctions, Fick's first law was interpreted as

$$I'(t) = D(C_{\mathcal{S}\mathrm{m}}(t) - C_{\mathcal{R}\mathrm{m}}(t)), \tag{A4}$$

where $I(t)$ is the intensity of the recovering cell and $C_{\mathcal{R}\mathrm{m}}(t)$ and $C_{\mathcal{S}\mathrm{m}}(t)$ are the concentrations of mobile fluorophores in the recovering cell and the supply cells, respectively. Diffusibility was compared by comparing estimates of D. A term accounting for the loss of fluorescence by means other than the gap junctions, e.g., fading of the fluorophores and diffusion through non-gap-junctional membrane, could have been added to Eq. (A4). However, positive controls indicated that fading was minimal over the 4-min measurement interval [13], and therefore such a term was not included.

Peters has analyzed the case in which $C_{\mathcal{S}\mathrm{m}}(t)$ is assumed to be constant [23]. This is equivalent to assuming a constant concentration of immobile fluorophores, $C_{\mathrm{Rt}}(0)$, over the time interval the recovery is observed. Under this assumption $C_{\mathcal{R}}(\infty) = C_{\mathcal{S}\mathrm{m}}(-) + C_{\mathcal{R}\mathrm{f}}(0)$. Thus

$$\begin{aligned} C_{\mathcal{S}\mathrm{m}}(t) - C_{\mathcal{R}\mathrm{m}}(t) &= C_{\mathcal{S}\mathrm{m}}(-) - C_{\mathcal{R}\mathrm{m}}(t) + C_{\mathcal{R}\mathrm{f}}(0) - C_{\mathcal{R}\mathrm{f}}(0) \\ &= C_{\mathcal{R}}(\infty) - C_{\mathcal{R}}(t), \end{aligned}$$

and Eq. (A4) reduces to

$$I'(t) = D(C_{\mathcal{R}}(\infty) - C_{\mathcal{R}}(t)). \tag{A5}$$

Equation (A2), equivalently Eq. (A3), is the solution to Eq. (A5), and a and k may be found by either Peters' technique [23] or a nonlinear least squares fitting procedure [18]. In this case the diffusion coefficient is recovered from k, because $k = rD/v$ where v is the volume of the cell and r is the proportionality constant relating intensity and the quantity of fluorophores. However, Zimmerman and Rose showed, using a dye injection method to study coupling between gap junctions, that there may be a loss of mobile fluorophores during the recovery phase [39].

In this study a model was developed to account for the loss of mobile fluorophores during the recovery phase of gap FRAP. Let $Q_m(t) = v \cdot C_{\mathcal{R}\mathrm{m}}(t)$ and $Q_f(t) = v \cdot C_{\mathcal{R}\mathrm{f}}(t)$ be the quantity of mobile and immobile fluorophores, respectively, in the bleached cell. Then the intensity of the bleached cell is $I(t) = (1/r)\mathrm{Q}(t) = ((1/r)Q_m(t) + Q_f(t))$, and Eq. (A4) may be written as

$$I'(t) = \frac{rD}{v}\left(\frac{v}{r} C_{\mathcal{S}\mathrm{m}}(t) - I(t) + \frac{1}{r} Q_f(t)\right),$$

and therefore,

$$I'(0) = \frac{rD}{v}\left(\frac{v}{r}(C_{\mathcal{S}\mathrm{m}}(0) + C_{\mathcal{R}\mathrm{f}}(0)) - I(0)\right).$$

Since, just after bleaching, the concentration of mobile fluorophores on the supply side is equal to the concentration of mobile fluorophores on the bleached side before bleaching, (letting $C_{\mathcal{R}}(-)$ be the concentration of fluorophores on the bleached side before it is bleached) $C_{\mathcal{R}m}(-) = C_{\mathcal{S}\mathrm{m}}(0)$. Thus,

$$\begin{aligned} &I'(0) \\ &= \frac{rD}{v}\left(\frac{v}{r}(C_{\mathcal{R}}(-) + C_{\mathcal{R}\mathrm{f}}(-) + C_{\mathcal{R}\mathrm{f}}(0) - C_{\mathcal{R}\mathrm{f}}(-)) - I(0)\right) \\ &= \frac{rD}{v}(I(-) - I(0)) - \frac{rD}{v}(I_f(-) - I_f(0)). \end{aligned}$$

Thus, letting $I_f(t)$ denote the intensity of the bleached cell due to the fixed fluorophores and using the relation $I_f(0) = I_f(-)(I(0)/I(-))$,

$$\frac{I'(0)}{I(0)} = \frac{rD}{v}\left[\frac{I(-) - I(0)}{I(0)} - \frac{I_f(-)}{I(-)}\left[\frac{I(-) - I(0)}{I(0)}\right]\right]$$
$$= \left[\frac{rD}{v} - \frac{I_f(-)}{I(-)}\right]\left[\frac{I(-) - I(0)}{I(0)}\right]. \quad \text{(A6)}$$

If the ratio of immobile fluorophores to mobile fluorophores is sufficiently small, then

$$\frac{I'(0)}{I(0)} \approx \frac{rD}{v}\left[\frac{I(-) - I(0)}{I(0)}\right], \quad \text{(A7)}$$

and the diffusion coefficient is obtained from the instantaneous rate of recovery at the time of the first postbleach scan and the fraction of bleaching. Therefore, if two cells are bleached by the same proportion, then identifying the systems with subscripts 1 and 2, letting D_i be the proportionality constant of Eq. (A3), and assuming equal volumes

$$\frac{I_1'(0)/I_1(0)}{I_2'(0)/I_2(0)} = \frac{D_1}{D_2}. \quad \text{(A8)}$$

If this assumption is not valid and if the fraction of immobile fluorophores at the time of the first postbleach scan is known, then Eq. (A6) can be used to obtain the diffusion coefficient.

Once the parameters a and k of Eq. (A3) have been estimated, the model recovery curve can be used to estimate the instantaneous rate of recovery

$$\frac{I'(t)}{I(t)} = \frac{ake^{-kt}}{a(1 - e^{-kt}) + I(0)/I(-)}. \quad \text{(A9)}$$

This is derived as follows. From Eq. (A1),

$$I(t) = \frac{\mathrm{PR}(t) \cdot I(-)}{100} + I(0) \quad \text{(a)}$$

(substituting Eq. (A2) into (a))

$$= a(1 - e^{-kt}) \cdot I(-) + I(0). \quad \text{(b)}$$

Differentiating (b) yields

$$I'(t) = I(-) \cdot k \cdot a \cdot e^{-kt}. \quad \text{(c)}$$

Equation (A9) is the quotient (c)/(b).

Provided the cell systems have been bleached by equal percentages, and the concentration of immobile fluorophores is sufficiently small, ratios of the diffusion constants, for different cell systems, can be calculated as ratios of a times k. Evaluating Eq. (A9) at $t = 0$ yields

$$\frac{I'(0)}{I(0)} = a \cdot k \cdot \frac{I(-)}{I(0)}. \quad \text{(A10)}$$

Then, using subscripts to distinguish the parameters for two different systems which have been bleached by equal percentages, a combination of Eqs. (A8) and (A10) (assuming cells of equal volumes) yields

$$\frac{D_1}{D_2} = \frac{a_1 k_1}{a_2 k_2}. \quad \text{(A11)}$$

Equation (A11) provides a means of analyzing diffusion through gap junctions in cell systems which do not recover to the same percentage of the prebleach level and for which there is continued immobilization of the fluorophores during the recovery period. When the cell systems are initially bleached to the same level and recover to the same level $a_1 = a_2$, and Eq. (A11) reduces to

$$\frac{D_1}{D_2} = \frac{k_1}{k_2}. \quad \text{(A12)}$$

Relative diffusion through gap junctions using gap FRAP data has previously been measured by comparing the recovery after a given time interval, i.e., $\mathrm{PR}_1(t)/\mathrm{PR}_2(t)$, where t is often taken to be one or more minutes following the first postbleach scan [13, 19, 22, 36–38]. The ratio of the percent recoveries after a given time interval (an average rate of recovery) is an approximation to the ratio of the instantaneous rates of recovery at the time of the first postbleach scan if the cell systems are bleached by equal percentages. Precisely,

$$\lim_{t \to 0}\left(\frac{\mathrm{PR}_1(t)}{\mathrm{PR}_2(t)}\right) = \frac{I_1'(0)/I_1(0)}{I_2'(0)/I_2(0)}. \quad \text{(A13)}$$

REFERENCES

1. Nicolson, G. L. (1982) *Biochim. Biophys. Acta* **695,** 113–176.
2. Weinstein, R. S., and Pauli, B. U. (1987) *Ciba Found. Symp.* **125,** 240–260.
3. Garrod, D. R., Parrish, E. P., and Marston, J. E. (1987) *Biochemical Soc. Trans.* **15,** 802–804.
4. Staehelin, L. A. (1974) *Int. Rev. Cytol.* **39,** 191–278.
5. McNutt, N. S., Hershberg, R. A., and Weinstein, R. S. (1971) *J. Cell Biol.* **51,** 805–825.
6. Green, K. J., Stappenbeck, T. H., Noguchi, S., Oyasu, R., and Nilles, L. A. (1991) *Exp. Cell Res.* **193,** 134–143.
7. Kocher, O., Amaudruz, M., Schindler, A. M., and Gabbiani, G. (1981) *J. Submicrosc. Cytol.* **13,** 267–281.
8. Ren, J., Hamada, J., Takeichi, N., Fujikawa, S., and Kobayashi, H. (1990) *Cancer Res.* **50,** 358–362.

9. Dervan, P. A., Gilmartin, L. G., Johnston, P. G., and Desmond, C. N. (1988) *Am. J. Surg. Pathol.* **12,** 855-860.
10. Komitowski, D., Kett, P., Janson, C., and Jarsch, E. D. (1989). *Pathol. Res. Pract.* **185,** 621-624.
11. Johnson, R., Hammer, M., Sheridan, J., and Revel, J. P. (1974) *Proc. Natl. Acad. Sci. USA* **71,** 4536-4540.
12. Loewenstein, W. R. (1981) *Physiol. Rev.* **61,** 829-913.
13. Stein, L. S., Stoica, G., Tilly, R., and Burghardt, R. C. (1991) *Cancer Res.* **51,** 696-706.
14. Jones, J. C. R., and Goldman, R. D. (1985) *J. Cell Biol.* **101,** 506-517.
15. Stein, L. S., Welsh, T. H., Wilson, V. G., and Burghardt, R. C. (1992) *In Vitro Cell. Dev. Biol.* **28A,** 436-444.
16. Boyer, B., Tucker, G. C., Valles, A. M., Franke, W. W., and Thiery, J. P. (1989) *J. Cell Biol.* **109,** 1495-1509.
17. Wade, M. A., Trosko, J. E., and Schindler, M. (1986) *Science* **232,** 525-528.
18. Stein, L. S., Boonstra, J., and Burghardt, R. C. (1992) *Exp. Cell Res.* **198,** 1-7.
19. de Feijter, A. W., Ray, J. S., Weghorst, C. M., Klaunig, E., Goodman, J. I., Chang, C. C., Ruch, R. J., and Trosko, J. E. (1990). *Mol. Carcinog.* **3,** 54-67.
20. Weidner, K. M., Behrens, J., Vandekerckhove, J., and Birchmeier, W. (1990) *J. Cell Biol.* **111,** 2097-2108.
21. Schindler, M., Trosko, J. E., and Wade, M. H. (1987) *Methods Enzymol.* **141,** 439-447.
22. Dookwah, H. D., Barhoumi, R., Narasimhan, T. K., Safe, S. H., and Burghardt, R. C. (1992) *Biol. Reprod.* **47,** 397-406.
23. Peters, R. (1984) *Eur. Biophys. J.* **11,** 43-50.
24. Priestly, M. B. (1981) Spectral Analysis and Time Series (Birnbaum, Z. W., and Lukacs, E., Eds.), pp. 89-90, Academic Press, London.
25. Burt, J. M. (1991) *in* Biophysics of Gap Junction Channels. (Peracchia, C., Ed), pp. 75-93, CRC Press, Boca Raton, FL.
26. Franke, W. W., Grund, C., Kuhn, C., Jackson, B. W., and Illmensee, K. (1982) *Differentiation* **20,** 43-59.
27. Jones, C. R., and Grelling, K. A. (1989) *Cell Motil. Cytoskeleton* **13,** 181-194.
28. Czernobilsky, B., Moll, R., Leppien, G., Schweikhart, G., and Franke, W. W. (1987) *Am. J. Pathol.* **126,** 476-486.
29. Valles, A. M., Boyer, B., Badet, J., Tucker, G. C., Barritault, D., and Thiery, J. P. (1990) *Proc. Natl. Acad. Sci. USA* **97,** 1124-1128.
30. DiSaia, P. J., and Creasman, W. J. (1989) *in* Clinical Gynecologic Oncology (Bircher, J., Ed.), pp. 325-416, Mosby, Washington, DC.
31. Copeland, L. J. (1991) *in* Gynecologic Oncology, Treatment Rationale and Techniques. (Greer, B. E., and Berek, J. S., Eds.), pp. 3-12, Elsevier, New York.
32. Legan, P. K., Collins, J. E., and Garrod, D. R. (1992) *BioEssays* **14,** 385-393.
33. Behrens, J., and Birchmeier, W., Goodman, S. L., and Imhof, B. A. (1985) *J. Cell Biol.* **101,** 1307-1315.
34. Matsuzaki, F., Mege, R. M., Jaffe, S. H., Friedlander, D. R., Gallin, W. J., Goldberg, J. I., Cunningham, B. A., and Edelman, G. M. (1990) *J. Cell Biol.* **110,** 1239-1252.
35. Mitchison, J. M. (1971) The Biology of the Cell Cycle, Cambridge Univ. Press, London.
36. Hasler, C. M., Frick, M. A., Bennink, M. R., and Trosko, J. E. (1990) *Toxicol. Appl. Pharmacol.* **103,** 389-398.
37. McKarns, S. C., and Doolittle, D. J. (1991). *Toxicol. Appl. Pharmacol.* **111,** 58-68.
38. Redmer, D. A., Grazul-Bilska, A. T., and Reynolds, L. P. (1991) *Endocrinology* **91,** 2757-2766.
39. Zimmerman, A. L., Rose, B. (1985) *J. Membr. Biol.* **84,** 269-283.
40. Crank, J. (1990) The Mathematics of Diffusion, pp. 2-5, Oxford Univ. Press, New York.

Received December 11, 1992
Revised version received March 31, 1993